Response to Reviewer #2

Reviewer #2 Comments and Suggestions for Authors:
The paper by Li et al. with the title "Tropospheric bromine monoxide in Ny-Ålesund: source analysis and impacts on the atmospheric chemistry" presented a comprehensive dataset, including BrO, ozone, aerosol, and mercury observations and modelled results. Bromine explosion is an old topic, but it still has many unknowns for the atmospheric research community. The paper has good in-depth new findings of both measurements and modelling work. I would support publishing this work if the authors could address my questions and concerns listed here.

Author's Response: We thank Reviewer #2 for the valuable comments, which greatly improve this manuscript. Please kindly find our point-by-point responses to the problems/comments below in blue, and changes to the manuscript in orange.

Major comments:

Q2.1: Line 25-26: This is a misleading claim. Contacting time does not necessarily mean contributions to BEEs. The longer contact with multi-year sea ice only suggests the possibility, but can not be used as a conclusive reason. Multi-year sea ice has lower salinity has been viewed as less possible as a major bromine source. To support this argument, more analysis is needed. E.g., can the increase in BrO signals from GOME be linked to the multi-year ice area? How can we rule out that 23.8% contact with first-year ice is not the real major contributor to the bromine? Some analysis, such as extreme cases, might help. E.g., if you can find any case that is only in contact with multi-year sea ice.

A2.1: We thank the reviewer for this important and constructive comment. We agree that air-mass contact time with a given surface type does not directly quantify its contribution to bromine explosion events (BEEs). We have revised the corresponding sentence to clarify that longer contact with multi-year sea ice (MYI) indicates a potential rather than a conclusive contribution to BEEs. As suggested, a representative BrO enhancement case was added to the revised version to demonstrate the importance of MYI, as shown below.

This BEE, occurring between the afternoon of 1 April 2020 and 3 April 2020 over Ny-Ålesund, was captured by both GOME-2B satellite observations and ground-based MAX-DOAS measurements (Fig. 1, Fig. 2b-d). This BEE was also well captured by p-TOMCAT model (Fig. 1).
To investigate the source regions of this BrO enhancement, we performed analyses for surface meteorological conditions (Fig. 2e-l) and ran 5-day backward trajectories arriving at Ny-Ålesund at 10 m, 200 m, and 500 m altitude, with results shown alongside the sea ice distribution (Fig. 2m-p). As shown, this BEE is associated with an approaching low-pressure system moving from the central Arctic (Fig. 2e-h). Under this system, air masses over the MYI were constrained by Greenland's topography and experienced enhanced surface winds (Fig. 2i-l). Before the low-pressure system approached Ny-Ålesund (ahead of 12:00 1 April), air masses

were mainly from first-year sea ice (FYI) (Fig. 2m-n), where no significant BrO enhancements were measured despite strong winds. However, when air masses passed over the MYI (as shown in Fig. 2o), enhanced BrO was detected. The same case was also reported in Zilker et al. (2023), who performed FLEXPART-WRF backward trajectory analyses of near-surface air masses arriving at Ny-Ålesund on 2 April 2020 at 11:00 UTC. Their 0–50 m backward analysis showed that particles arriving at Ny-Ålesund originated mainly from the northern MYI-covered regions. This suggests that the enhanced BrO observed at Ny-Ålesund is likely related to the transport of reactive bromine associated with sea-salt aerosols produced over MYI.

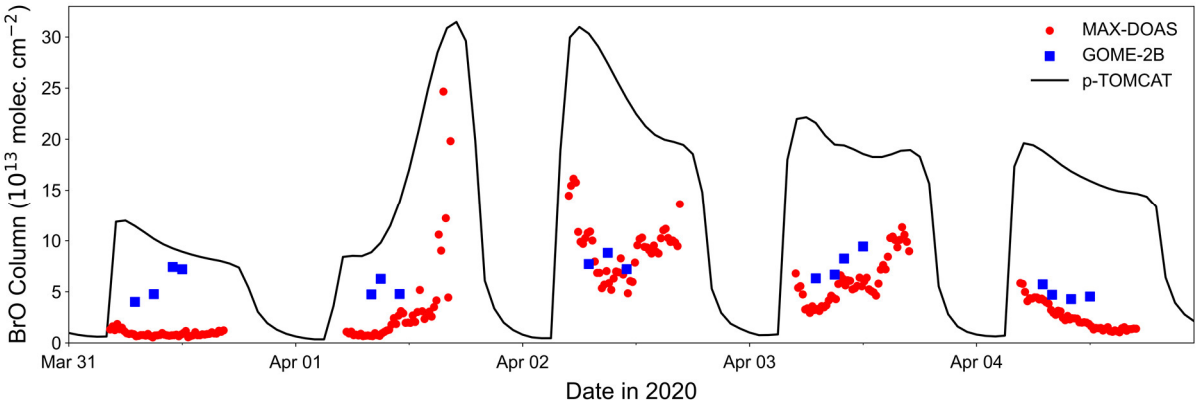

Figure 1. MAX-DOAS BrO partial columns (red scatters), GOME-2B tropospheric BrO columns (blue scatters) and p-TOMCAT BrO partial columns (black line) between 31 March and 4 April in 2020 at Ny-Ålesund.

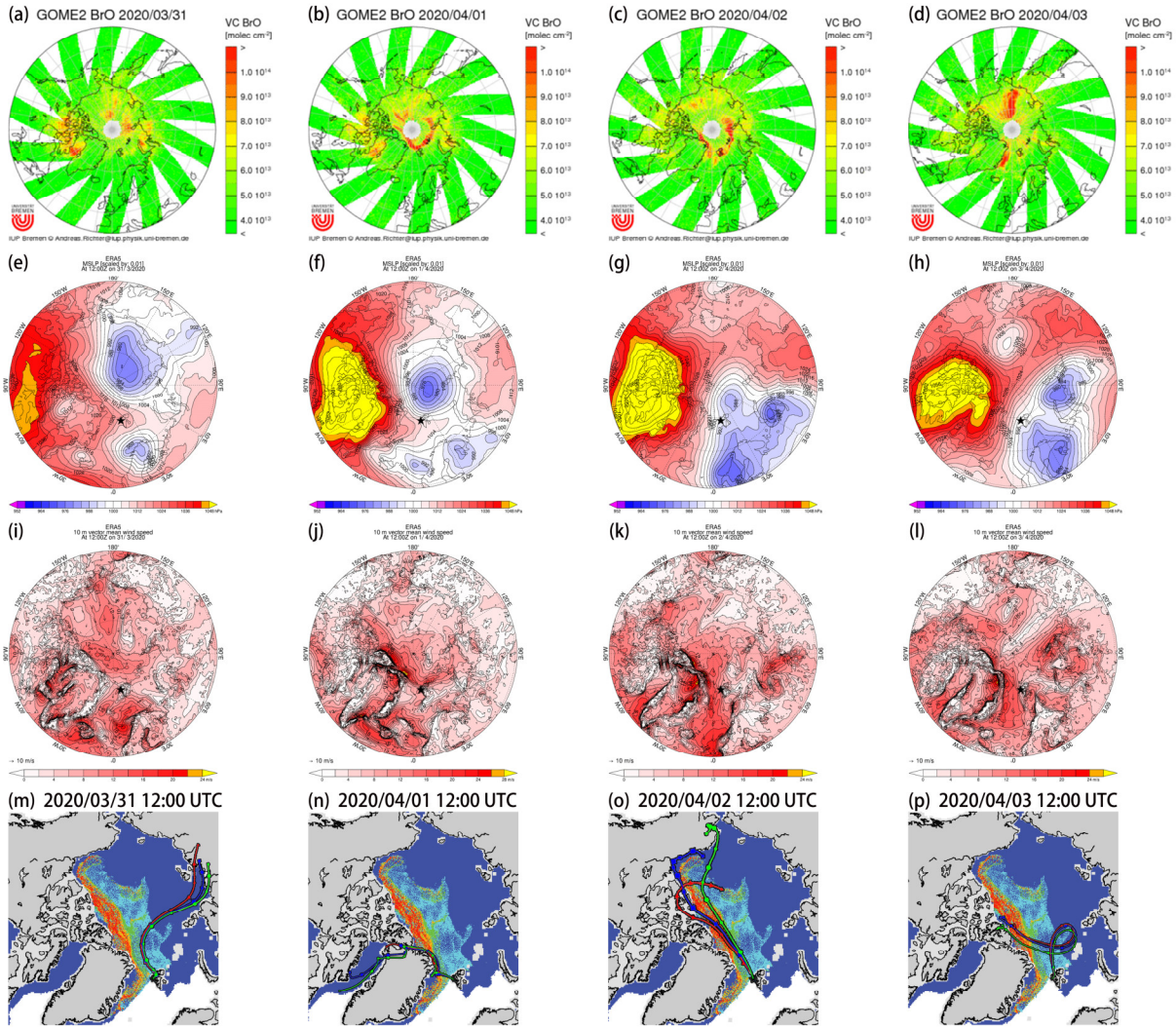

Figure 2. (a, b, c, d) GOME-2B tropospheric BrO columns; (e, f, g, h) Mean sea level pressure; (i, j, k, l) wind speed; (m, n, o, p) Air mass trajectories at 10 m (red line), 200 m (blue line), and 500 m (green line) combined with sea ice, from 31 March 2020, 12:00 UTC to 3 April 2020, 12:00 UTC in Ny-Ålesund.

Furthermore, we derived wind speed distributions over MYI and FYI for all BEEs (2017–2023) based on 5-day backward trajectories. Figure 3 shows that during BEEs, air masses generally take about 2.4 times longer contact time over MYI than over FYI across the full wind-speed range (0–30 m s^{-1}). For wind speeds exceeding 7 m s^{-1}, air masses generally take about 2.8 times longer contact time over MYI (41522 h) than over FYI (14886 h).

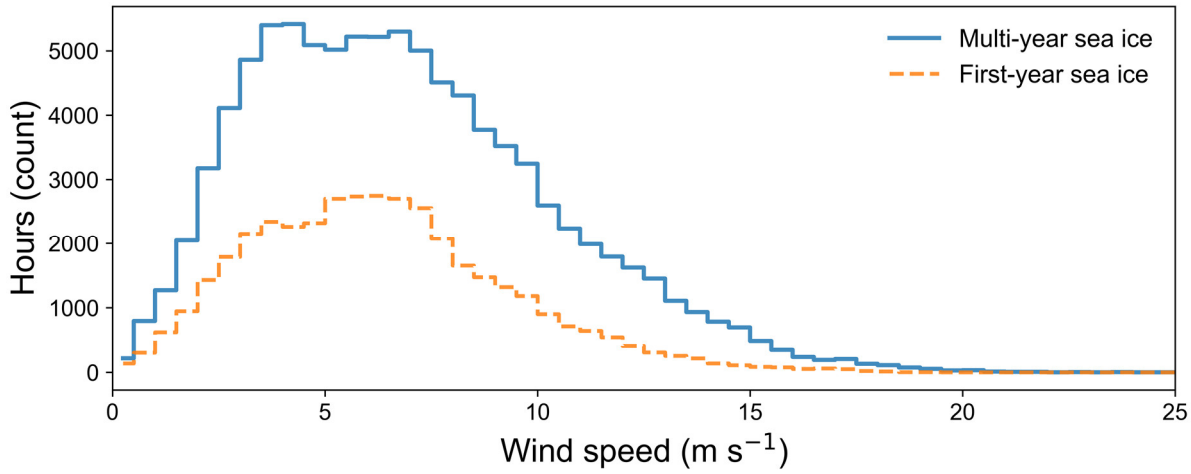

Figure 3. Wind speed distributions along backward trajectories of air masses arriving at Ny-Ålesund during BEEs, separated by trajectory segments over MYI and FYI. The distribution represents combined statistics for March–May during 2017–2023, expressed as the total number of hours in each wind-speed bin.

The corresponding section of the manuscript has been modified as below:

3.5 Potential role of MYI in BEEs

To further investigate the importance of MYI to BEEs, we present a representative case study of BrO enhancement. This BEE, occurring between the afternoon of 1 April 2020 and 3 April 2020 over Ny-Ålesund, was captured by both GOME-2B satellite observations and ground-based MAX-DOAS measurements as well as p-TOMCAT model (Fig. 12, Fig. 13b-d). This BEE event was also well captured by p-TOMCAT model (Fig. 12).

To investigate the source regions of this BrO enhancement, we performed analyses for surface meteorological conditions (Fig. 13e-l) and ran 5-day backward trajectories arriving at Ny-Ålesund at 10 m, 200 m, and 500 m altitude, with results shown alongside the sea ice distribution (Fig. 13m-p). As shown, this BEE is associated with an approaching low-pressure system moving from the central Arctic (Fig. 13e-h). Under this system, air masses over the MYI were constrained by Greenland's topography and experienced enhanced surface winds (Fig. 13i-l). Before the low-pressure system approached Ny-Ålesund (ahead of 12:00 1 April), air masses were mainly from FYI (Fig. 13m-n), where no significant BrO enhancements were measured despite strong winds. However, when air masses passed over the MYI (as shown in Fig. 13o), enhanced BrO was detected. The same case was also reported in Zilker et al. (2023), who performed FLEXPART-WRF backward trajectory analyses of near-surface air masses arriving at Ny-Ålesund on 2 April 2020 at 11:00 UTC. Their 0–50 m backward analysis showed that particles arriving at Ny-Ålesund originated mainly from the northern MYI-covered regions. This suggests that the enhanced BrO observed at Ny-Ålesund is likely related to the transport of reactive bromine associated with sea-salt aerosols produced over MYI.

Furthermore, we derived wind speed distributions over MYI and FYI for all BEEs (2017–2023) based on 5-day backward trajectories. Figure 14 shows that during BEEs, air masses generally take about 2.4 times longer contact time over MYI than over FYI across the full wind-speed range (0–30 m s^{-1}). For wind speeds exceeding 7 m s^{-1}, air masses generally take about 2.8

times longer contact time over MYI (41522 h) than over FYI (14886 h).

Zilker, B., Richter, A., Blechschmidt, A.-M., von der Gathen, P., Bougoudis, I., Seo, S., Bösch, T., and Burrows, J. P.: Investigation of meteorological conditions and BrO during ozone depletion events in Ny-Ålesund between 2010 and 2021, Atmos. Chem. Phys., 23, 9787–9814, https://doi.org/10.5194/acp-23-9787-2023, 2023.

Q2.2: Line 57-59: since your major finding is that multi-year sea ice plays important role than first-year sea ice, more descriptions of current understandings and previous findings on these two sources should be provided. What are the differences between first and multi-year sea ice in terms of bromine chemistry? If they are both considered as sources, are they considered on a similar or different level in the BEE contributions?

A2.2: We added a new paragraph in the Introduction Part (shown below) to summarise our current understanding and previous findings regarding FYI and MYI as potential bromine sources.

"FYI and MYI differ in their physical and chemical properties, which may influence the efficiency of bromine activation. MYI is generally thicker and less porous than FYI, and these physical characteristics limit brine connectivity within the ice and its upward transport, resulting in distinct roles in Arctic bromine chemistry (Haas et al., 2006, 2010). After undergoing multiple summer melt–refreeze cycles, MYI is desalinated through gravity drainage and flushing, whereas FYI typically retains higher salinity (Krnavek et al., 2012). Although brine can migrate upward through the ice–snow interface and supply salts to overlying snow, this process is highly sensitive to snow depth, with observations suggesting an effective upper limit of approximately 17 cm (Domine et al., 2004). MYI regions generally accumulate deeper snowpacks, limiting the upward transport of salts from the ice and resulting in lower snow salinity compared to FYI (Webster et al., 2014; Blanchard-Wrigglesworth et al., 2015). Under such low-salinity conditions, atmospheric deposition and recycling may become increasingly important in controlling bromide availability in the snow (Krnavek et al., 2012; Nandan et al., 2017). Surface snow over MYI typically exhibits low salinity, with typical median value around 0.01 practical salinity unit (psu), whereas snow over FYI is generally more saline, with median values ranging from 0.1 to 0.7 psu (Krnavek et al., 2012). Analysis of bromine enrichment factors indicates that bromide depletion is more frequently observed in snow over MYI compared to snow over FYI, suggesting that, in addition to FYI, MYI may actively participate in Arctic boundary layer bromine chemistry (Peterson et al., 2019). This explains the enhanced tropospheric BrO observed over MYI regions (Peterson et al., 2016; Burd et al., 2017). Further modeling studies suggest that blowing-snow–sourced sea-salt aerosol emissions from MYI regions may contribute approximately 20–30% of Arctic springtime tropospheric BrO enhancement, indicating that MYI represents a significant source of bromine activation (Huang et al., 2020). A recent field measurement in the high Arctic coastal area (Yang et al., 2024) provide evidence for the dominant role of atmospheric processes in controlling surface-layer bromide concentrations. For example, snow samples collected from offshore and onshore sites during early springtime at Eureka, Canada, show

very low salinities in the snow skin layer (<1 cm), with corresponding bromide enriched by up to a factor of 10, suggesting the importance of atmospheric deposition processes. As a result, they could serve as a direct source of reactive bromine once lifted by winds, even though the corresponding salinity is very low. Current chemistry models do not take this effect into account."

Blanchard-Wrigglesworth, E., Farrell, S. L., Newman, T., and Bitz, C. M.: Snow cover on Arctic sea ice in observations and an Earth System Model, Geophys. Res. Lett., 42, 10,342–10,348, https://doi.org/10.1002/2015GL066049, 2015.

Burd, J. A., Peterson, P. K., Nghiem, S. V., Perovich, D. K., and Simpson, W. R.: Snowmelt onset hinders bromine monoxide heterogeneous recycling in the Arctic, J. Geophys. Res. Atmos., 122, 8297–8309, https://doi.org/10.1002/2017JD026906, 2017.

Domine, F., Sparapani, R., Ianniello, A., and Beine, H. J.: The origin of sea salt in snow on Arctic sea ice and in coastal regions, Atmos. Chem. Phys., 4, 2259–2271, https://doi.org/10.5194/acp-4-2259-2004, 2004.

Haas, C., Hendricks, S., and Doble, M.: Comparison of the sea-ice thickness distribution in the Lincoln Sea and adjacent Arctic Ocean in 2004 and 2005, Ann. Glaciol., 44, 247–252, https://doi.org/10.3189/172756406781811781, 2006.

Haas, C., Hendricks, S., Eicken, H., and Herber, A.: Synoptic airborne thickness surveys reveal state of Arctic sea ice cover, Geophys. Res. Lett., 37, L09501, https://doi.org/10.1029/2010GL042652, 2010.

Huang, J., Jaeglé, L., Chen, Q., Alexander, B., Sherwen, T., Evans, M. J., Theys, N., and Choi, S.: Evaluating the impact of blowing-snow sea salt aerosol on springtime BrO and O3 in the Arctic, Atmospheric Chemistry and Physics, 20, 7335–7358, https://doi.org/10.5194/acp-20-7335-2020, 2020.

Krnavek, L., Simpson, W. R., Carlson, D., Domine, F., Douglas, T. A., and Sturm, M.: The chemical composition of surface snow in the Arctic: Examining marine, terrestrial, and atmospheric influences, Atmos. Environ., 50, 349–359, https://doi.org/10.1016/j.atmosenv.2011.11.033, 2012.

Nandan, V., Geldsetzer, T., Yackel, J., Mahmud, M., Scharien, R., Howell, S., King, J., Ricker, R., and Else, B.: Effect of Snow Salinity on CryoSat-2 Arctic First-Year Sea Ice Freeboard Measurements, Geophys. Res. Lett., 44, 10419–10426, https://doi.org/10.1002/2017GL074506, 2017.

Peterson, P. K., Simpson, W. R., and Nghiem, S. V.: Variability of bromine monoxide at Barrow, Alaska, over four halogen activation (March–May) seasons and at two on-ice locations, J. Geophys. Res. Atmos., 121, 1381–1396, https://doi.org/10.1002/2015JD024094, 2016.

Peterson, P. K., Hartwig, M., May, N.W., Schwartz, E., Rigor, I., Ermold, W., Steele, M., Morison, J. H., Nghiem, S. V., and Pratt, K. A.: Snowpack measurements suggest role for multi-year sea ice regions in Arctic atmospheric bromine and chlorine chemistry, Elem. Sci. Anth., 7, 14, https://doi.org/10.1525/elementa.352, 2019.

Webster, M. A., Rigor, I. G., Nghiem, S. V., Kurtz, N. T., Farrell, S. L., Perovich, D. K., and Sturm, M.: Interdecadal changes in snow depth on Arctic sea ice, J. Geophys. Res. Oceans., 119, 5395–5406, https://doi.org/10.1002/2014JC009985, 2014.

Yang, X., Strong, K., Criscitiello, A. S., Santos-Garcia, M., Bognar, K., Zhao, X., Fogal, P.,

Walker, K. A., Morris, S. M., and Effertz, P.: Surface snow bromide and nitrate at Eureka, Canada, in early spring and implications for polar boundary layer chemistry, Atmos. Chem. Phys., 24, 5863–5886, https://doi.org/10.5194/acp-24-5863-2024, 2024.

In this study, snow salinity over FYI is based on MOSAiC measurements (Macfarlane et al., 2023); over MYI, half the FYI salinity is applied, which accounts for the two opposing effects: lower snow salinity but higher bromine enrichment. As shown in Figure 4, the calculated blowing-snow-sourced bromine emissions during 2017-2023 BEEs indicate that bromine flux over MYI accounts for an average of 54% (35–67%) of total bromine flux over sea ice.

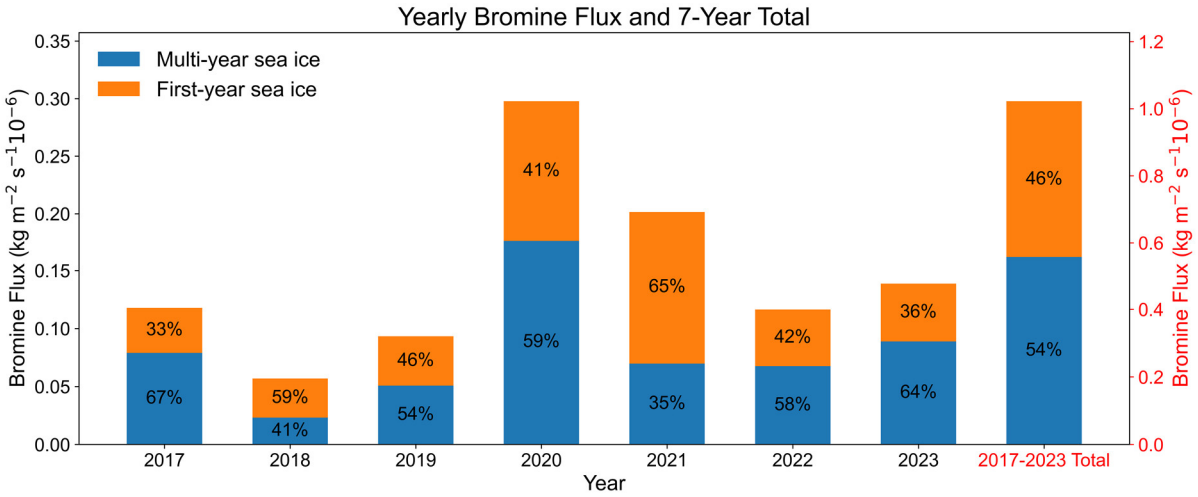

Figure 4. Yearly (March–May) and seven-year total blowing-snow-sourced bromine emission fluxes over MYI and FYI along backward trajectories of air masses arriving at Ny-Ålesund during BEEs. Blue and orange bars indicate the contributions from MYI and FYI, respectively.

The corresponding section of the manuscript has been modified as below:

"Snow salinity values over FYI used in the study were obtained from the MOSAiC measurements (Macfarlane et al., 2023); over MYI, half the FYI salinity is applied, which accounts for the two opposing effects: lower snow salinity but higher bromine enrichment. As shown in Figure S2, the calculated blowing-snow-sourced bromine emissions during 2017-2023 BEEs indicate that bromine flux over MYI accounts for an average of 54% (35–67%) of total bromine flux over sea ice."

Macfarlane, AR, Schneebeli, M, Dadic, R, Tavri, A, Immerz, A, Polashenski, C, Krampe, D, Clem ens-Sewall, D, Wagner, DN, Perovich, DK, Henna-Reetta, H, Raphael, I, Matero, I, Regnery, J, Smith, MM, Nicolaus, M, Jaggi, M, Oggier, M, Webster, MA, Lehning, M, Kolabutin, N, Itkin, P, Naderpour, R, Pirazzini, R, Ha¨mmerle, S, Arndt, S, Fons, S.: A database of snow on sea ice in the central Arctic collected during the MOSAiC expedition. Scientific Data, 10, 398, http:// dx.doi.org/10.1038/s41597-023-02273-1, 2023.

Q2.3: Line 118-124: I understand this is a complicated research topic and the background is rich. The author did a good job of providing some background. However, I still read that the

introduction part is not well organized. E.g., the author talked about the general features of studies of BEE first, then discussed the local observations from Ny-Ålesund. In this part, they go back to the other field findings again.

A2.3: We have reorganized the structure of the introduction accordingly, e.g. by moving the section on local observations from Ny-Ålesund to the penultimate paragraph. The new introduction flow from the general background on BEE to the specific local context.

Q2.4: Line 178: In March, I would expect the site still to have snow cover. Can the author explain why surface albedo is set to only 0.1? Even in the referenced paper, this 0.1 surface albedo is not specifically discussed. But, for satellite, typically 0.9 will be used for such conditions. Comments?

A2.4: Thank you for the comment. We note that in March, although the site itself may be snow-covered, the surrounding ocean is presented by open seawater due to the influence of the North Atlantic Warm Current.

For our ground-based MAX-DOAS analysis, we used the SCIATRAN software (Rozanov et al., 2005) to get the modeled differential Air Mass Factor (DAMF) at 2° elevation based on assumed BrO profiles with air masses distributed between 0–4 km, corresponding to the a priori profiles used in the profile retrievals. Figure 5 shows the modeled DAMF at 2° elevation at Ny-Ålesund in March as a function of solar zenith angle (SZA) under different surface albedo conditions. It can be seen that the DAMF does not change significantly with different surface albedo, with an average difference of approximately 1.8% between surface albedo values of 0.1 and 0.9. This is consistent with Wagner et al. (2007), who reported that, in contrast to satellite observations, ground-based MAX-DOAS sensitivity is almost independent of the surface albedo and hardly decreases at large SZAs. Therefore, using a surface albedo of 0.1 in our simulations has a negligible effect on the resulting DAMFs.

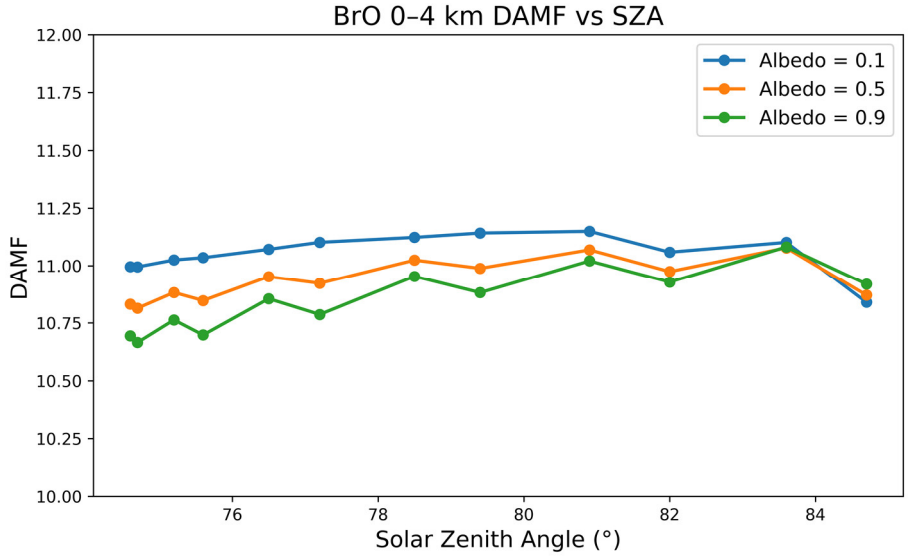

Figure 5. Modeled MAX-DOAS DAMF at 2° elevation at Ny-Ålesund in March as a function of SZA under different surface albedos (0.1, 0.5, 0.9).

The corresponding section of the manuscript has been modified as below:

"The surface albedo was set to 0.1 (Chen et al., 2022). In contrast to satellite observations, MAX-DOAS sensitivity is almost independent of the surface albedo and hardly decreases at large SZAs (Wagner et al., 2007)."

Chen, D., Luo, Y., Yang, X., Si, F., Dou, K., Zhou, H., Qian, Y., Hu, C., Liu, J., and Liu, W.: Study of an Arctic blowing snow-induced bromine explosion event in Ny-Alesund, Svalbard, Sci Total Environ, 839, 156335, https://doi.org/10.1016/j.scitotenv.2022.156335, 2022.

Rozanov, A., Bovensmann, H., Bracher, A., Hrechanyy, S., Rozanov, V., Sinnhuber, B.-M., Stroh, F., and Burrows, J. P.: NO_2 and BrO vertical profile retrieval from SCIAMACHY limb measurements: Sensitivity studies, Adv. Space Res., 36, 846–854, https://doi.org/10.1016/j.asr.2005.03.013, 2005.

Wagner, T., Ibrahim, O., Sinreich, R., Frieß, U., von Glasow, R., and Platt, U.: Enhanced tropospheric BrO over Antarctic sea ice in mid winter observed by MAX-DOAS on board the research vessel Polarstern, Atmos. Chem. Phys., 7, 3129–3142, https://doi.org/10.5194/acp-7-3129-2007, 2007.

Q2.5: Line 219-220: p-TOMCAT is driven by ERA5, while HYSPLIT is driven by GDAS. These datasets have different vertical, horizontal, and even temporal resolutions (6 hr vs. 1 hr). Any comments on the impact of different meteorological inputs? Since p-TOMCAT is a transport model, is it possible to directly analyze sea-ice contact information from p-TOMCAT simulations?

Line 263-268: Isn't such emission flux information part of the p-TOMCAT simulation results? If yes, what does it look like? If not, what are the main challenges here? Anyway, the point is that hybridizing results from a transport model with another trajectory model seems redundant and questionable (mainly, they are driven by different meteorological fields that have very different resolutions).

A2.5: The above two questions will be answered together here. Note that p-TOMCAT uses ERA5-based reanalysis data, while HYSPLIT uses GDAS data. In p-TOMCAT, the 6-hourly ERA5 meteorological fields at their native resolution (0.25° × 0.25°) are regridded to a coarse horizontal resolution of 2.825° × 2.825° for use in the simulations. The p-TOMCAT output is archived at hourly intervals. GDAS provides 1° × 1° analyses every 6 hours, and HYSPLIT outputs hourly trajectories at 1° × 1° resolution.

Regarding the impact of different meteorological inputs, we acknowledge that differences in temporal and spatial resolution may affect the resulting transport and derived quantities. To investigate this, we compared bromine fluxes calculated from blowing snow along 5-day backward trajectories (1° × 1°), using the corresponding ERA5 meteorological data (0.25° × 0.25°, hourly) with the same parameterization as in the model, and with those obtained directly from p-TOMCAT's outputs. Figure 6 shows that bromine fluxes calculated directly from ERA5 data are approximately 2.8 times larger than those from p-TOMCAT for the period of March–

May 2020. The elevated flux in the ERA5 calculation is largely attributed to the high meteorological resolution, while the coarse model horizontal resolution may smooth out sub-grid meteorological variability. In addition, p-TOMCAT does not distinguish between MYI and FYI; areas where sea ice persisted through the preceding summer are treated as MYI, which contributes to the bias. For this reason, rather than taking the values directly from the model's outputs, we combined HYSPLIT backward trajectories with ERA5 meteorology and incorporated higher-resolution sea-ice conditions to directly derive bromine emission fluxes, which is essential for diagnosing spatially localized bromine emission fluxes.

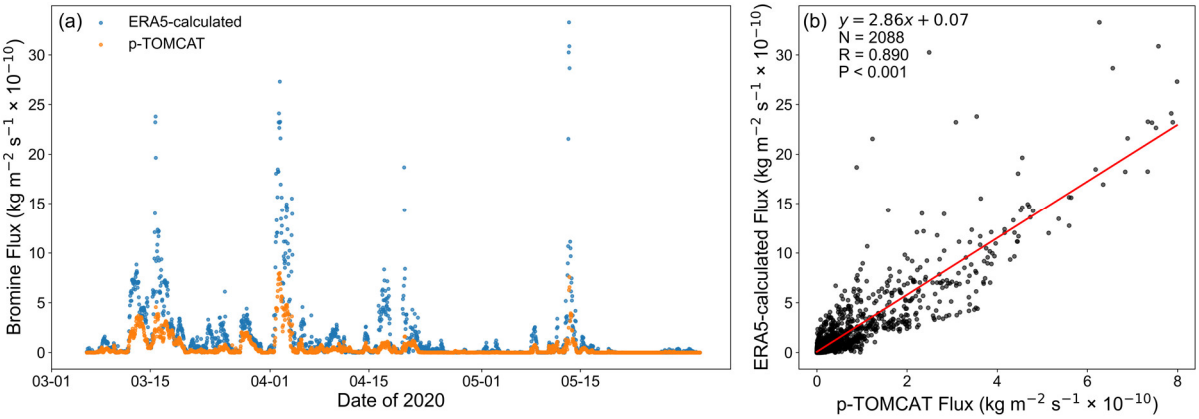

Figure 6. (a) Time series of blowing-snow-sourced bromine fluxes calculated from ERA5 meteorological fields (blue dots) and from the p-TOMCAT (orange dots) during March–May 2020. The fluxes are summed over the 0–3 km layer and shown at hourly resolution. (b) Scatter plot showing the correlation between the ERA5-calculated and p-TOMCAT-simulated blowing-snow-sourced bromine fluxes over the same period.

The corresponding section of the manuscript has been modified as below:

"In our simulations, ERA5 fields at their native horizontal resolution (0.25° × 0.25°) were first regridded to match the p-TOMCAT horizontal resolution (2.825° × 2.825°)."

"These bromine emission fluxes are not taken directly from p-TOMCAT model output; instead, they are calculated using native-resolution ERA5 meteorology along backward trajectories. In addition to p-TOMCAT's coarse horizontal resolution, monthly sea-ice coverage (Rayner et al., 2003) was used without distinguishing between MYI and FYI; areas where sea ice persisted through the preceding summer are therefore treated as MYI in a coarse approximation. As a result, p-TOMCAT cannot precisely distinguish fluxes between MYI and FYI, so the bromine emission fluxes are calculated using ERA5 meteorology. The comparison shows that blowing-snow-sourced bromine fluxes calculated directly from ERA5 can be 2–3 times larger than those from p-TOMCAT outputs, which is likely due to differences in meteorological resolution and sea-ice representation (see Figure S3 in the Supplement)."

Rayner, N. A., Parker, D. E., Horton, E. B., Folland, C. K., Alexander, L. V., Rowell, D. P., Kent, E. C., and Kaplan, A.: Global analyses of sea surface temperature, sea ice, and night marine air temperature since the late nineteenth century, Journal of Geophysical Research: Atmospheres, 108, 4407, https://doi.org/10.1029/2002jd002670, 2003.

Yang, X., Pyle, J. A., and Cox, R. A.: Sea salt aerosol production and bromine release: Role of snow on sea ice, Geophys. Res. Lett., 35, L16815, https://doi.org/10.1029/2008gl034536, 2008.

Q2.6: Figure 5: The general n-shape curve for the number of profiles in Fig 5a and 5c is reasonable. But why Fig 5e show double peaks?

A2.6: The double-peak structure mainly arises from the combined effects of the seasonal evolution of the SZA sampling range and the temporal variation of SZA, as illustrated by the following analysis. Figure 7 shows the SZA distributions corresponding to the actual MAX-DOAS observation times. When all observation times are considered, the SZA distributions in March and April exhibit a single peak, whereas May clearly shows a double-peak structure. This difference is closely related to the seasonal evolution of sunlight conditions in spring. Specifically, the observable SZA range gradually expands over the course of each month: in early March, SZA is mostly within 84–86°, extending to 74–86° by late March; in early April, it spans 74–86°, further extending to 64–86° by late April; while in May, the SZA range exhibits approximately 62–86° in early May and 56–80° in late May. As a result, in May, the distribution of observation time points across SZA is no longer concentrated in a single range but forms two relatively distinct intervals.

Figure 8 highlights how SZA variation rates contribute to the double-peak structure. For example, during morning observations in May, the two SZA intervals around 78–80° and 62–64° correspond to the peaks. The first reason is that observations from both early and late May cover these two intervals, providing sufficient data points in each. The second reason, as shown in Figure 8c, is that SZA changes relatively slowly within these intervals, allowing the instrument to remain longer and accumulate more valid observations. Together, these factors lead to the double peaks in the statistical distribution.

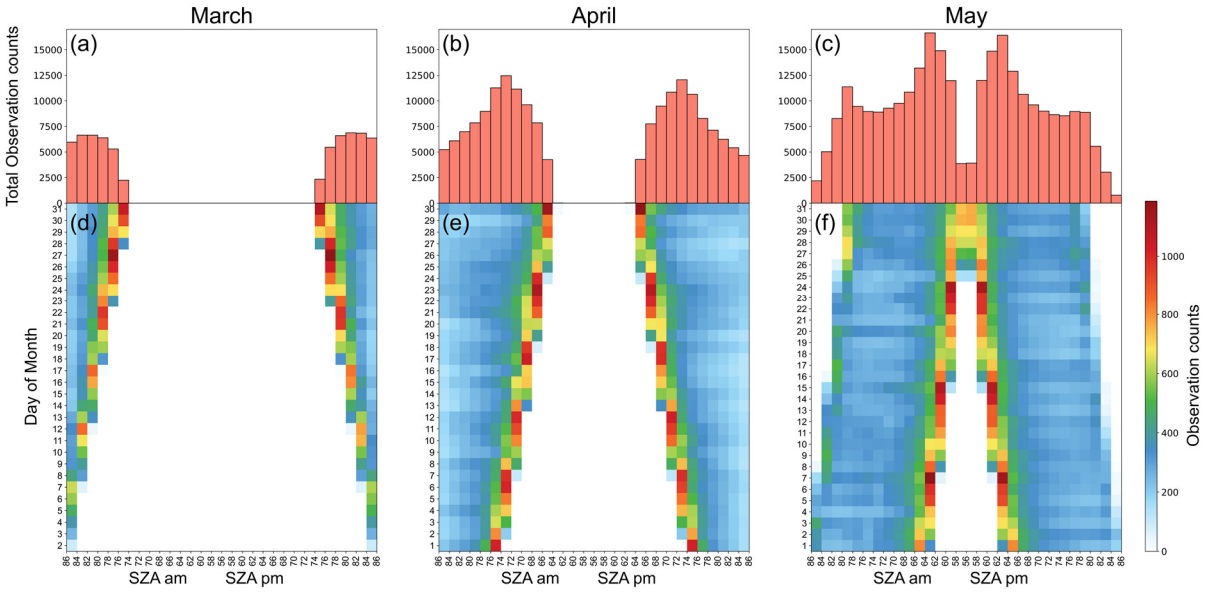

Figure 7. SZA distributions sampled at the times of MAX-DOAS measurements during March (a, d), April (b, e), and May (c, f) in 2017–2023. Panels (a–c) show the total number of observations aggregated across all years as a function of SZA for

morning (AM) and afternoon (PM) conditions, while panels (d–f) present the corresponding daily SZA frequency distributions. March and April are characterized by a single peak at large SZA, whereas May exhibits clear double peaks.

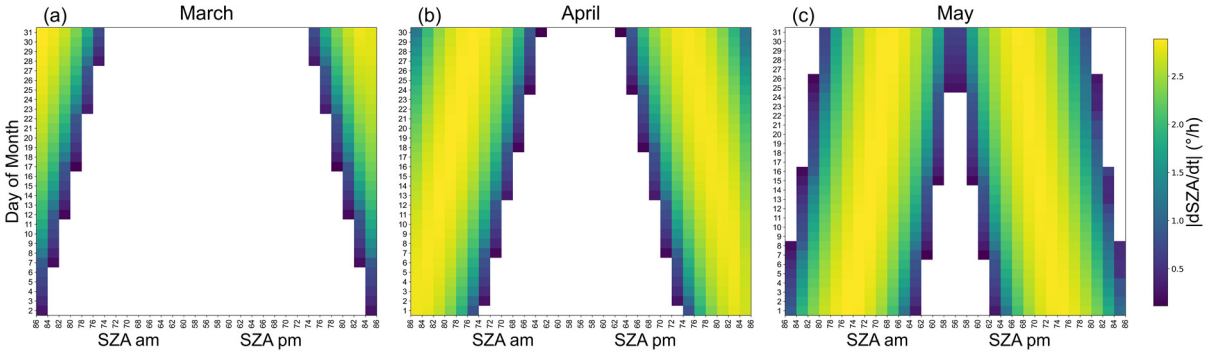

Figure 8. Absolute SZA variation rates (|dSZA/dt|, °/h) sampled at the times of MAX-DOAS measurements in March (a), April (b), and May (c) during 2017–2023. For each day, morning (AM) and afternoon (PM) observations are binned by SZA. Different colors represent the value of |dSZA/dt|, with lower values corresponding to slower SZA variation and higher values to faster SZA variation.

The corresponding section of the manuscript has been modified as below:

"In addition, The double-peak structure (Fig. 5e) in May mainly arises from the seasonal expansion of the observable SZA range and the slower SZA variation at specific SZA intervals, which leads to enhanced sampling at two distinct SZA ranges (78°–80° and 62°–64°; see Figs. S4 and S5)."

Q2.7: Line 368-369: Does this "sea ice contacting time" include both multi-year and first-year sea ice? Please make this clear. Also, if yes, can you break down the sea ice contact time into multi-year and first-year sea ice?

Figures 6 and 7: as the author claimed in the abstract and conclusion that one key finding is that multi-year sea ice plays a key role, I would expect the panels to have "sea ice contact time," meaning the contact with multi-year sea ice (not just all types of sea ice). Please make this clear in the captions and the related discussion part.

A2.7: The above two questions will be answered together here. In the original manuscript (Lines 368–369), the term "sea ice contact time" referred to the total sea ice contact time, including both MYI and FYI. We have now clarified this in the revised manuscript.

Specifically, the back-trajectory-based analysis shows that BrO is significantly positively correlated with total sea ice contact time ($r = 0.48$, $p < 0.0001$), whereas no significant correlation is found with open ocean contact time ($r = -0.02$, $p = 0.145$). Additionally, we find that BrO also exhibits a positive correlation with MYI contact time ($r = 0.47$, $p < 0.0001$), and a weaker but still statistically significant correlation with FYI contact time ($r = 0.22$, $p < 0.0001$).

In response, we have revised the figures and captions to clearly distinguish between total sea ice, MYI, and FYI contact times. The Figures 6 and 7 in the original manuscript have been updated and are now presented as Figures 9 and 10 in this response.

In addition, we have revised the corresponding description in the main text.

"BrO and aerosol extinction profiles, MYI, FYI, total sea ice, and open ocean contact along air mass history trajectories, surface ozone, gaseous mercury, BrO partial column, and key meteorological parameters are presented in Fig. 6."

"Moving to the back-trajectory-based analysis, BrO shows a significant positive correlation with total sea ice contact time (including both MYI and FYI; $r = 0.48$, $p < 0.0001$), whereas no significant correlation is found with open ocean contact time ($r = -0.02$, $p = 0.145$). When separated by ice type, BrO exhibits a statistically significant positive correlation with MYI contact time ($r = 0.47$, $p < 0.0001$), stronger than its correlation with FYI ($r = 0.22$, $p < 0.0001$)."

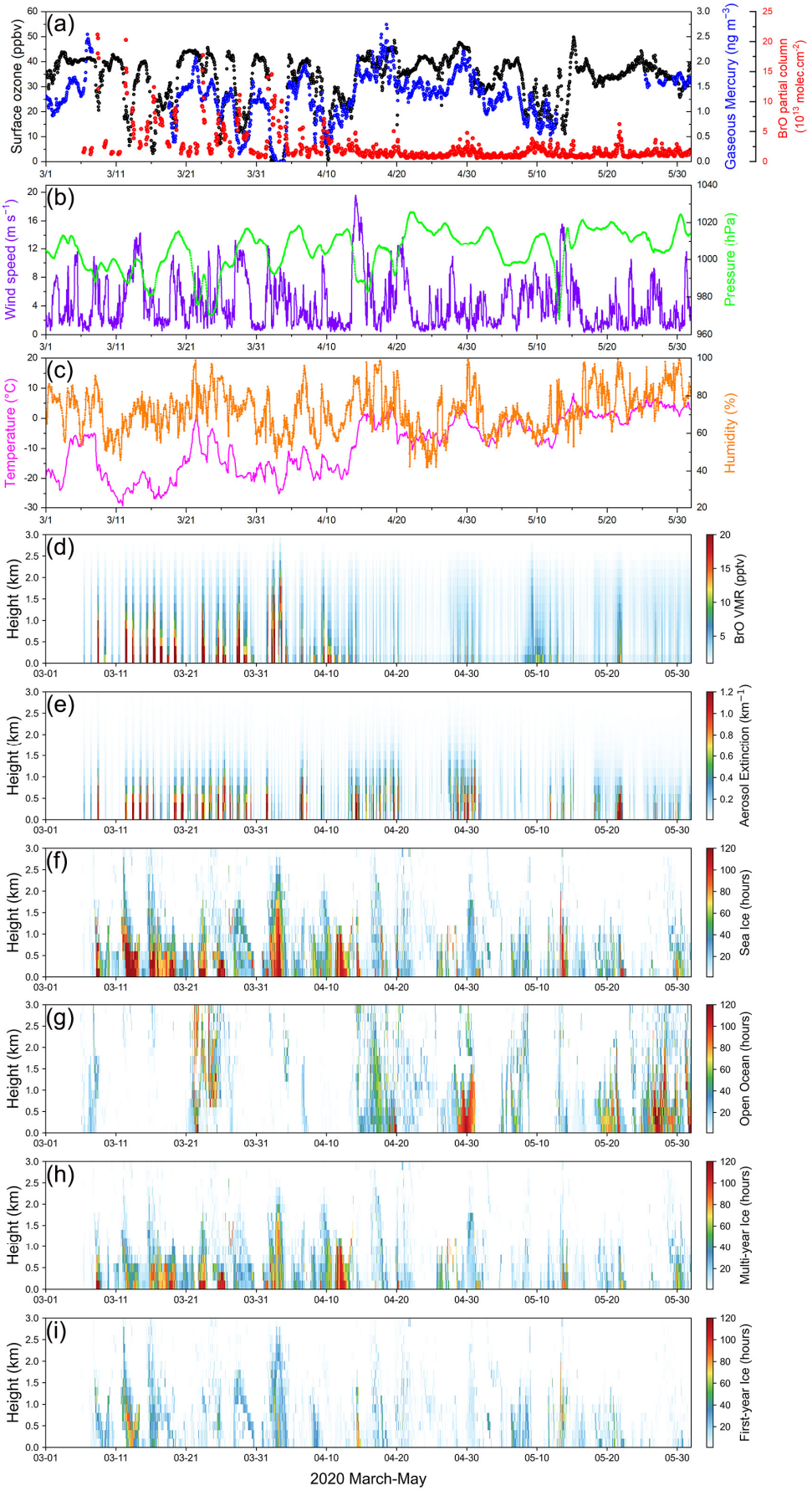
(a)
Surface ozone (ppbv)
Gaseous Mercury (ng m^{-3})
BrO partial column (10^{13} molec.cm^{-2})
(b)
Wind speed (m s^{-1})
Pressure (hPa)
(c)
Temperature (°C)
Humidity (%)
(d)
Height (km)
BrO VMR (pptv)
(e)
Aerosol Extinction (km^{-1})
(f)
Sea Ice (hours)
(g)
Open Ocean (hours)
(h)
Multi-year Ice (hours)
(i)
First-year Ice (hours)
3/1
3/11
3/21
3/31
4/10
4/20
4/30
5/10
5/20
5/30
03-01
03-11
03-21
03-31
04-10
04-20
04-30
05-10
05-20
05-30
2020 March-May

Figure 9. Panel (a) surface ozone (black dots), gaseous mercury (Hg(0)) (blue dots) and BrO partial column (red dots); (b) wind speed (purple line), pressure (green line); (c) temperature (pink line), relative humidity (orange line); (d) BrO profiles; (e) aerosol extinction profiles; (f) total sea ice contact time profiles; (g) open ocean contact time profiles; (h) MYI contact time profiles; and (i) FYI contact time profiles between March and May 2020 in Ny-Ålesund. All data are shown at hourly resolution.

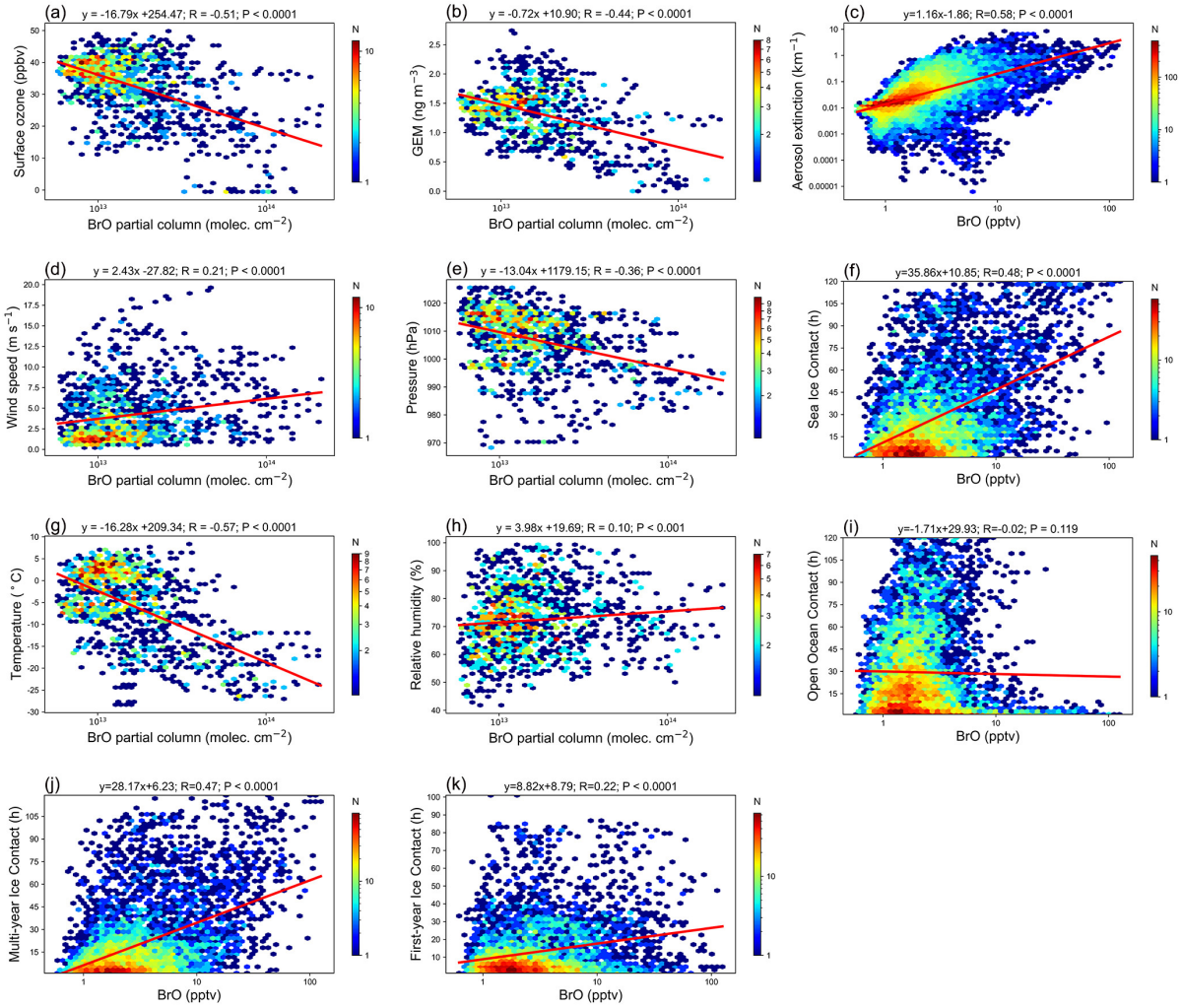

Figure 10. Correlation analysis between BrO and various parameters during March–May 2020. BrO partial column correlations are shown for surface ozone (a), GEM (b), wind speed (d), pressure (e), temperature (g), and relative humidity (h). BrO VMR profile correlations are shown for aerosol profiles (c), total sea ice contact time (f), open ocean contact time (i), MYI contact time (j), and FYI contact time (k).

Q2.8: Line 430-436 and 492-495: My understanding is that the BEE in p-TOMCAT is mainly driven by this SSA production mechanism. But, here it seems the author also wants to emphasize the role of multi-year sea ice. What kind of role does the multi-year sea ice play in p-TOMCAT's bromine simulation? I am not against the hypothesis, but is it possible to quantify the emissions from SSA and multi-year sea ice? I understand this could not be easy, but currently, the description is very tangled and confusing. Or maybe the author is suggesting blowing snow on multi-year sea ice is more productive than blowing snow on one-year sea ice? The correlation between modelled BrO and contact time with different sea ice types is very low, and their difference (0.17-0.29 vs. 0.03-0.23) is very small. This is not a good support for

the argument in lines 494-495.

A2.8: Thanks for the comment. In the current model's configuration, snow salinity over FYI is based on MOSAiC measurements (Macfarlane et al., 2023), while snow over MYI is assigned half the FYI salinity. As described in A2.5, the sea-ice dataset used in the model can not distinguish between FYI and MYI, and the derived "multi-year" sea ice based on summertime ice is approximate and unreliable. Therefore, the estimated bromine fluxes in p-TOMCAT are not robust or quantitatively meaningful; we are planning to investigate this issue in a more reliable UK Earth System Model.

As shown in Fig 3 and 4, more reliable back-trajectory calculations indicate that air masses spend 2.4 times over MYI than over FYI during BEEs. As a result, MYI accounts for more than half of the cumulative bromine flux, underscoring the important role of MYI in BEEs at Ny-Ålesund.

BrO variability is controlled by multiple factors, including both physical and chemical processes; contact time with the underlying surface is just one of them. Therefore, it is not surprising to see relatively small correlation coefficients between them. Anyway, the data indicate the importance of MYI, which was previously thought to be less important. In the revised manuscript, we have rephrased the sentence as shown below:

"In addition, BrO is positively correlated with both FYI and MYI from March to May, with correlation coefficients between BrO and contact time with MYI (0.17–0.29, $p < 0.0001$) slightly higher than those with FYI (0.03–0.23). These indicate that MYI could play an important role, as FYI does, in determining BEEs at Ny-Ålesund."

Macfarlane, AR, Schneebeli, M, Dadic, R, Tavri, A, Immerz, A, Polashenski, C, Krampe, D, Clem ens-Sewall, D, Wagner, DN, Perovich, DK, Henna-Reetta, H, Raphael, I, Matero, I, Regnery, J, Smith, MM, Nicolaus, M, Jaggi, M, Oggier, M, Webster, MA, Lehning, M, Kolabutin, N, Itkin, P, Naderpour, R, Pirazzini, R, Ha¨mmerle, S, Arndt, S, Fons, S.: A database of snow on sea ice in the central Arctic collected during the MOSAiC expedition. Scientific Data, 10, 398, http:// dx.doi.org/10.1038/s41597-023-02273-1, 2023.

Q2.9: Technical issues:
Line 140: Some information, such as the distance between the Arctic Yellow River Station and Zeppelin Station, should be provided.

A2.9: The horizontal distance between the Arctic Yellow River Station in Ny-Ålesund (78.92° N, 11.93° E) and the Zeppelin Station (78.90° N, 11.88° E) is approximately 2.1 km, based on their geographic coordinates (Platt et al., 2022). This has been added to the manuscript.

"Continuous ozone and GEM measurements have been carried out at Zeppelin Station (78.90° N, 11.88° E; 472 m asl), located approximately 2.1 km from the Arctic Yellow River Station (Platt et al., 2022)."

Platt, S. M., Hov, Ø., Berg, T., Breivik, K., Eckhardt, S., Eleftheriadis, K., Evangeliou, N., Fiebig, M., Fisher, R., Hansen, G., Hansson, H.-C., Heintzenberg, J., Hermansen, O., Heslin-Rees, D., Holmén, K., Hudson, S., Kallenborn, R., Krejci, R., Krognes, T., Larssen, S., Lowry, D., Lund Myhre, C., Lunder, C., Nisbet, E., Nizzetto, P. B., Park, K.-T., Pedersen, C. A., Aspmo Pfaffhuber, K., Röckmann, T., Schmidbauer, N., Solberg, S., Stohl, A., Ström, J., Svendby, T., Tunved, P., Tørnkvist, K., van der Veen, C., Vratolis, S., Yoon, Y. J., Yttri, K. E., Zieger, P., Aas, W., and Tørseth, K.: Atmospheric composition in the European Arctic and 30 years of the Zeppelin Observatory, Ny-Ålesund, Atmos. Chem. Phys., 22, 3321–3369, https://doi.org/10.5194/acp-22-3321-2022, 2022.